Influence of the Self-Interference Channel Model on the Performance of a Full-Duplex MIMO System

Xuan Chen, Vincent Savaux, Matthieu Crussière, Patrick Savelli, Kofi-Clément Yao

Influence of the Self-Interference Channel Model on the Performance of a Full-Duplex MIMO System

Xuan Chen*†‡, Vincent Savaux*, Matthieu Crussière†, Patrick Savelli* and Kofi-Clément Yao§
*b<>com, 1219 Av. des Champs Blancs, 35510 Cesson-Sévigné, France
†Univ. Rennes, INSA Rennes, CNRS, IETR UMR-6164, F-35700 Rennes, France
‡TDF, 155 bis Av. Pierre Brossolette, 92120 Montrouge, France
§Lab-STICC, CNRS, UMR 6285, UBO 29238 Brest, France

***Abstract*—In this paper, we study the behavior of a multiple-input multiple-output (MIMO) full-duplex (FD) system according to two different models of the self-interference (SI) channel inherent to the FD communication strategy: the spherical wave model (SWM) and the planar wave model (PWM). More precisely, we evaluate the received SI power at the receiver antenna array by changing the relative geometrical position of the transmitter antenna array in respect to the latter. Our study shows a significant difference between the two models. In particular we theoretically show as well as through simulation that the SWM for the SI channel is more precise than the PWM, and should then be considered for practical applications of the FD concept.**

***Index Terms*—Analog beamforming, full-duplex, MIMO, planar wave model, self-interference, spherical wave model.**

I. Introduction

These last decades, full-duplex (FD) has been proven to be one of the most appealing but also most challenging communication technologies [1]–[5]. The main advantage of FD is its capacity to transmit and receive different signals at the same time. Thus, it becomes theoretically possible for FD devices to double the spectral efficiency compared to half-duplex (HD) devices. However, FD devices suffer from the presence of self-interference (SI) that inevitably occurs since the transmitter (TX) is likely to radiate in the direction of the co-localised receiver (RX), while the receiver is trying to receive a signal from other devices.

For any FD system to work properly the management of the SI becomes the most important task to deal with. One of the key factors for the design of an efficient self-interference cancellation (SIC) technique is the model of the SI channel. Most of the existing works dealing with FD systems model the SI channel with a planar wave model (PWM), e.g. [6]–[8], which is not rigorously correct taking into account the short distance between the transmitter and the receiver antenna parts. Thus, it seems more relevant to consider the spherical wave model (SWM) which is expected to reveal more precisely the short distance propagation effects. This becomes even more critical considering transmit and receive radiating devices in the form of antenna arrays, since the size of the radiating disposal is hereby augmented. Recently more and more authors start to question the use of the PWM while modelling the SI channel in FD systems. In [9] and [10], the authors do consider the SWM for the SI channel model, however no solid theoretical proof was provided to justify the latter consideration. In [11], the authors adopted the SWM for the SI channel model, however limiting the work to the case of a uniform linear arrays (ULA). This limiting case finally showed very few advantage in favor of the SWM model compared to its PWM counterpart.

In this paper, we consider a generic MIMO FD system with the capacity of analog beamforming, and we propose to analyze and compare the system performance between the PWM and SWM models. Unlike [11], we consider in our work a uniform planar array (UPA) structure instead of a ULA, to fully exhibit the potential advantage of SWM compared to PWM. In particular, we first demontrate that the received SI power evaluated upon the PWM model can be written in a simplified way whereas such a simplification is not possible if the SWM model is used. This proves that the SWM model is much more generic and accurate than the PWM model to characterize the behavior of the SI link in FD systems. To confirm this fact, we then provide simulation results of a realistic FD system with various relative positions of the antenna arrays. Our experiments clearly show the lack of accuracy of the PWM approximation making the SWM model essential in the perspective of proper SIC algorithm design for FD systems and more generally FD performance assessment.

The rest of the paper is organized as follows: Section II introduces the PWM and SWM channel models and our considered FD MIMO system model as well as the analog beamforming model, section III provides the justification of the validity domain of PWM and the theoretical analysis involving the PWM model, section IV gives the simulation results while section V concludes our work.

Notations: Boldface letters $\boldsymbol{a}$ and normal font letters a represent vectors and scalars, respectively. Capital boldface letters $\mathbf{A}$ represents matrix. $\boldsymbol{A}^H$ represents the conjugate transpose operation of matrix $\boldsymbol{A}$. $\|.\|_2$ denotes the L2-norm.

II. Channel Model and System Model

In this section we first present the considered MIMO FD system model. We then introduce the two channel models we consider: the PWM and the SWM. The end of this section presents the analog beamforming model we consider in our work.

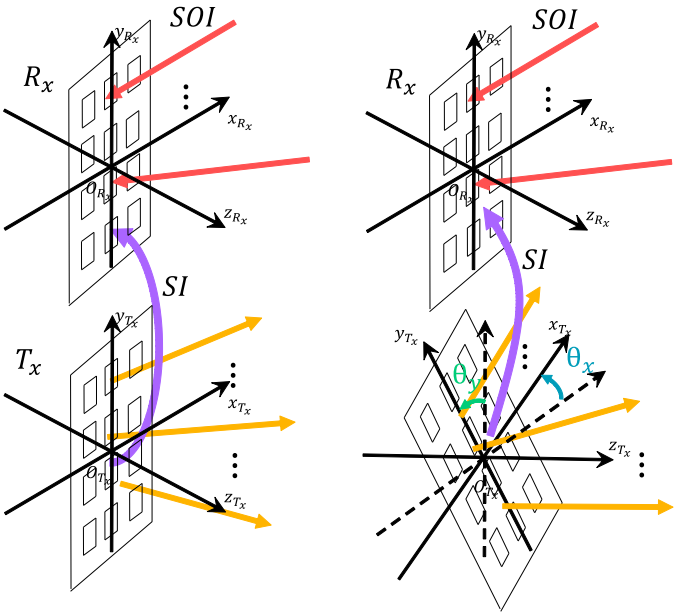

Fig. 1. 3D view of the relative position change of the TX array to the RX array.

A. System Model

In our work we consider a generic FD MIMO system with a TX part and a RX part. Each part has its own antenna array dedicated to transmit signals to other devices or receive signals of interest (SOI) from other devices, and each antenna array has its own number of antennas M_t for TX and M_r for RX. We assume that both TX and RX arrays are built in the same way: both adopt the UPA structure with a $\frac{\lambda}{2}$ spacing between adjacent elementary antennas. Without loss of generality we assume that the TX array is placed closely below the RX array. Fig. 1 shows the topology for both TX and RX arrays. A Cartesian orthonormed coordinated system (O_i, x_i, y_i, z_i) with $i \in \{R_x, T_x\}$ is associated to each array. Initially the two coordinated systems are exactly the same with a translation along the y axis between each other as shown in the left part of Fig. 1. During our study, we consider that the position of the TX array can vary according to two angles as shown in the right part of Fig. 1: a tilt angle θ_x around the x axis and θ_y around the y axis. We study the effect of these two angles on the received SI power radiated from the TX array on the RX array. The received signal at RX side can be written as:

$$\boldsymbol{y} = \boldsymbol{W}_{\mathrm{RF}}^{H} \boldsymbol{H}_{\mathrm{SI}} \boldsymbol{F}_{\mathrm{SI}} \boldsymbol{x}_{\mathrm{SI}} + \boldsymbol{y}_{\mathrm{SOI}} + \boldsymbol{W}_{\mathrm{RF}}^{H} \boldsymbol{n}, \tag{1}$$

with $\boldsymbol{y}$ the vector gathering all the received signal at the RX array, $\boldsymbol{W}_{\mathrm{RF}}$ the analog post coding matrix at RX side (detailed in the next section), $\boldsymbol{H}_{\mathrm{SI}}$ the SI channel between the RX array and the TX array using PWM or SWM, $\boldsymbol{F}_{\mathrm{RF}}$ the analog precoding matrix at TX side, $\boldsymbol{x}_{\mathrm{SI}}$ the vector gathering all the signals sent from the TX array which represent precisely the source of SI for the RX array, $\boldsymbol{y}_{\mathrm{SOI}}$ the vector gathering all the SOI for RX and $\boldsymbol{n}$ the vector gathering the noise received at each elementary antenna of the RX array.

B. Spherical wave model

The SI channel coefficient with SWM between the m-th ($\forall m \in \{0, \ldots, M_r - 1\}$) receiver antenna and the n-th ($\forall n \in \{0, \ldots, M_t - 1\}$) transmitter antenna can be defined as in the work of [12]:

$$h_{\mathrm{SI},m,n} = \rho e^{j\phi} \frac{D}{D_{m,n}} e^{-j\frac{2\pi}{\lambda}\Delta_{m,n}^{\mathrm{SWM}}}, \tag{2}$$

with $\rho e^{j\phi}$ the complex gain expressing the channel between the center O_{T_x} of the TX antenna array and the center O_{R_x} of the RX antenna array, $\frac{D}{D_{m,n}}$ an amplitude fluctuation term due to the small distance between the TX and RX antennas, where D is the distance between O_{T_x} and O_{R_x} and $D_{m,n}$ is the distance between the centre of the m-th antenna of the receiver antenna array and the centre of the n-th antenna of the transmitter antenna array, λ the wavelength and $\Delta_{m,n}^{\mathrm{SWM}} \triangleq D_{m,n} - D$ the phase shift with respect to the reference points located at O_{T_x} and O_{R_x} defined as:

$$\Delta_{m,n}^{\mathrm{SWM}} = \| -\boldsymbol{a}_{t,n} + D\boldsymbol{u}_t + R\boldsymbol{a}_{r,m} \|_2 - D, \tag{3}$$

with $-\boldsymbol{a}_{t,n}$ (resp. $\boldsymbol{a}_{r,m}$) the vector from the n-th (resp. m-th) antenna of the TX (resp. RX) array to the centroid O_{T_x} (resp. O_{R_x}), $D\boldsymbol{u_t}$ the vector from O_{T_x} to O_{R_x} (with $\boldsymbol{u}_t$ the unitary vector pointing from O_{T_x} to O_{R_x}), $\boldsymbol{R}$ the rotation matrix mapping the vectors of the RX coordinate into the TX coordinate: $\boldsymbol{R}\boldsymbol{u}_r = -\boldsymbol{u}_t$ and $\boldsymbol{u}_r$ the dual vector of $\boldsymbol{u}_t$ for the RX array.

C. Planar Wave Model

The PWM corresponds to the first order term in the Taylor development of the expression of SWM and so the SI channel can be defined as follows:

$$\boldsymbol{H}_{\mathrm{SI}}^{\mathrm{PWM}} = \sqrt{M_t M_r} \rho e^{j\phi} \boldsymbol{e}_r(\boldsymbol{u}_r) \boldsymbol{e}_t(\boldsymbol{u}_t)^H, \tag{4}$$

with $\rho e^{j\phi}$ the complex gain as defined in (2), $\boldsymbol{e}_r$ and $\boldsymbol{e}_t$ the steering vectors associated with the elementary antennas of the RX array and the TX array respectively. The steering vector can then be defined in a classic way as:

$$\boldsymbol{e}_x(\boldsymbol{u}_x) = \sqrt{\frac{1}{M_x}} \begin{bmatrix} e^{-j\frac{2\pi}{\lambda}\boldsymbol{a}_{x,0}\cdot\boldsymbol{u}_x} \\ \vdots \\ e^{-j\frac{2\pi}{\lambda}\boldsymbol{a}_{x,N_x-1}\cdot\boldsymbol{u}_x} \end{bmatrix}, \tag{5}$$

with $x \in \{t, r\}$.

D. Analog Beamforming Model

We adopt in our work the structure of partially connected RF chain to form the precoding/post coding matrix, which means the RF chains of the same unit (TX or RX) are independent from each other, and each RF chain is only connected to a unique sub-array of elementary antennas. Thus, each sub-array of elementary antennas has the capability to form a unique

directional beam, the latter being controlled by an array of phase shifters for example. In this sense, the analog precoding matrix $\boldsymbol{F}_{\mathrm{RF}}$ of size $M_t \times N_t^{\mathrm{RF}}$ can be formed by concatenating the steering vectors defined in (5) as:

$$\boldsymbol{F}_{\mathrm{RF}} = \begin{bmatrix} \boldsymbol{e}_0 & 0 & \cdots & 0 \\ 0 & \boldsymbol{e}_1 & \cdots & 0 \\ \vdots & \vdots & \ddots & \vdots \\ 0 & \cdots & \cdots & \boldsymbol{e}_{N_t^{\mathrm{RF}}-1} \end{bmatrix}, \tag{6}$$

with N_t^{RF} the number of RF chains at the TX side. Similarly, the analog post coding matrix $\boldsymbol{W}_{\mathrm{RF}}$ of dimension $M_r \times N_r^{\mathrm{RF}}$ can be formed in the same way with N_r^{RF} the number of RF chains at the RX side.

III. Theoretical Analysis

A. Validity Domain

We first evaluate the validity domain of the PWM and the SWM. The validity domain of the PWM can be defined from [12] as follows:

$$\mathcal{D} \geq \frac{8R_f^2}{\lambda}, \tag{7}$$

with λ the wavelength and R_f the Fraunhofer distance defined as in [13]:

$$R_f = \frac{\pi}{4}\frac{D_{\max}^2}{\Phi\lambda}, \tag{8}$$

with $D_{\max}$ the maximum aperture of the elementary antenna, Φ the maximum tolerated phase error and λ the wavelength. In our work we employ the patch antennas whose maximum aperture is optimized and equal to 4.24mm as in the work of [14]. Furthermore, we place ourselves under typical 5G mmWave conditions with a central frequency of 28GHz, which leads to $\lambda = 10.77$mm. For $\Phi = \frac{\pi}{8}$ which is a classic consideration in literature, the Fraunhofer distance in our case is $R_f = 3.3603$mm, leading to $\mathcal{D} = 8.4423$mm for the validity distance of the PWM. For the considered MIMO FD system in which the two arrays are placed one next to each other, only a distance of $\frac{\lambda}{2} = 5.36$mm can be found between the two arrays, which is clearly below the validity domain of the PWM. Thus, we see the necessity to consider the SWM in a FD system with transmit and receive disposals close to each other. Note that the value of R_f considered here only gives an order of magnitude of the validity domain of SWM *i.e.* does not represent an absolute bound on the choice of P/SWM.

B. Channel Model Analysis

In this section we theoretically evaluate the effect of the considered analog beamforming techniques on the SI power when PWM is used for the SI channel model. The received SI power at the m-th RF chain with PWM can be written as:

$$P_{\mathrm{SI},m}^{\mathrm{PWM}} = \sum_{n=0}^{N_t^{\mathrm{RF}}-1} P_{t,n} \left| (\boldsymbol{W}_{\mathrm{RF}}^H \boldsymbol{H}_{\mathrm{SI}}^{\mathrm{PWM}} \boldsymbol{F}_{\mathrm{RF}})_{m,n} \right|^2, \tag{9}$$

with $P_{t,n}$ the transmit power of the n-th RF chain at the TX side. By replacing the expression of $\boldsymbol{W}_{\mathrm{RF}}$ and $\boldsymbol{F}_{\mathrm{RF}}$ by their definition as in (6), (9) becomes:

$$P_{\mathrm{SI},m}^{\mathrm{PWM}} = \sum_{n=0}^{N_t^{\mathrm{RF}}-1} P_{t,n} \left| \sum_{k'=0}^{M_t^{(n)}-1} \frac{1}{\sqrt{M_t^{(n)}}} e^{-j\frac{2\pi}{\lambda}\boldsymbol{a}_{t,k'}^{(n)}\boldsymbol{u}_t} \left(\sum_{k=0}^{M_r^{(m)}-1} \frac{1}{\sqrt{M_r^{(m)}}} e^{j\frac{2\pi}{\lambda}\boldsymbol{a}_{r,k}^{(m)}\boldsymbol{u}_r} \boldsymbol{H}_{\mathrm{SI},k,k'}^{\mathrm{PWM}} \right) \right|^2. \tag{10}$$

The channel coefficient of $\boldsymbol{H}_{\mathrm{SI}}^{\mathrm{PWM}}$ can be derived from (4) and is expressed as:

$$\boldsymbol{H}_{\mathrm{SI},k,k'}^{\mathrm{PWM}} = \rho e^{j\phi} e^{-j\frac{2\pi}{\lambda}(\boldsymbol{a}_{r,k}^{(m)}\boldsymbol{u}_r^{\mathrm{SI}} - \boldsymbol{a}_{t,k'}^{(n)}\boldsymbol{u}_t^{\mathrm{SI}})}. \tag{11}$$

Replacing (11) in (10) leads to:

$$P_{\mathrm{SI},m}^{\mathrm{PWM}} = \sum_{n=0}^{N_t^{\mathrm{RF}}-1} \frac{\rho P_{t,n}}{M_t^{(n)} M_r^{(m)}} \left| \sum_{k'=0}^{M_t^{(n)}-1} e^{-j\frac{2\pi}{\lambda}\boldsymbol{a}_{t,k'}^{(n)}(\boldsymbol{u}_t - \boldsymbol{u}_t^{\mathrm{SI}})} \left(\sum_{k=0}^{M_r^{(m)}-1} e^{j\frac{2\pi}{\lambda}\boldsymbol{a}_{r,k}^{(m)}(\boldsymbol{u}_r - \boldsymbol{u}_r^{\mathrm{SI}})} \right) \right|^2. \tag{12}$$

Since UPA are considered for the antenna arrays, we define w (resp. w') and h (resp. h') the horizontal antenna index and the vertical antenna index for the RX (resp. TX) with $w \in \{0, \ldots, k_w^{(m)} - 1\}$ (resp. $w' \in \{0, \ldots, k_w'^{(n)} - 1\}$), $h \in \{0, \ldots, k_h^{(m)} - 1\}$ (resp. $h' \in \{0, \ldots, k_h'^{(n)} - 1\}$) and $k_w^{(m)}$ (resp. $k_w'^{(n)}$) and $k_h^{(m)}$ (resp. $k_h'^{(n)}$) the number of antennas per row for the m-th RF chain of RX (resp. TX) and the number of antennas per column for the m-th RF chain of RX (resp. TX). Thus, the array index k (resp. k') of RX (resp. TX) can be replaced and written as $k = hk_w^{(m)} + w$ (resp. $k' = h'k_w'^{(n)} + w'$). Relying on such new index (k, w) and (k', w'), (12) can be further simplified:

$$P_{\mathrm{SI},m}^{\mathrm{PWM}} = \sum_{n=0}^{N_t^{\mathrm{RF}}-1} \frac{\rho P_{t,n}}{M_t^{(n)} M_r^{(m)}} \left| \sum_{h'=0}^{k_h'^{(n)}-1} \sum_{w'=0}^{k_w'^{(n)}-1} e^{-j\frac{2\pi}{\lambda}\boldsymbol{a}_{t,h'k_w'^{(n)}+w'}^{(n)}(\boldsymbol{u}_t - \boldsymbol{u}_t^{\mathrm{SI}})} \left(\sum_{h=0}^{k_h^{(m)}-1} \sum_{w=0}^{k_w^{(m)}-1} e^{j\frac{2\pi}{\lambda}\boldsymbol{a}_{r,hk_w^{(m)}+w}^{(m)}(\boldsymbol{u}_r - \boldsymbol{u}_r^{\mathrm{SI}})} \right) \right|^2. \tag{13}$$

Given that a $\frac{\lambda}{2}$ spacing is assumed in the construction of our UPAs for both RX and TX, the result of the scalar products $\boldsymbol{a}_{t,h'k_w'^{(n)}+w'}^{(n)}\boldsymbol{u_t}$ and $\boldsymbol{a}_{r,hk_w^{(m)}+w}^{(m)}\boldsymbol{u_r}$ are known from [15] and can be expressed as follows:

$$\boldsymbol{a}_{t,h'k_w'^{(n)}+w'}^{(n)}\boldsymbol{u_t} = \frac{\lambda}{2}(w\cos(\phi^{(n)})\sin(\theta^{(n)}) + h\sin(\phi^{(n)})), \tag{14}$$

and

$$\boldsymbol{a}^{(m)}_{r,hk_w^{(m)}+w}\boldsymbol{u_r} = \frac{\lambda}{2}(w\cos(\phi^{(m)})\sin(\theta^{(m)}) + h\sin(\phi^{(m)})). \tag{15}$$

Since we consider two rotation angles θ_x around the x axis first and then θ_y around the y axis, the expression of the global rotation matrix $\boldsymbol{R}$ can be defined as the following:

$$\boldsymbol{R} = \begin{bmatrix} \cos(\theta_y) & \sin(\theta_x)\sin(\theta_y) & \cos(\theta_x)\sin(\theta_y) \\ 0 & \cos(\theta_x) & -\sin(\theta_x) \\ -\sin(\theta_y) & \sin(\theta_x)\cos(\theta_y) & \cos(\theta_x)\cos(\theta_y) \end{bmatrix}. \tag{16}$$

Note that the order of rotation is important at this point. If the rotation along the y axis is performed first, the global rotation matrix $\boldsymbol{R}$ has a different expression which leads also to a different expression of $\boldsymbol{u}_t^{\mathrm{SI}}$. Moreover, since we suppose that only the TX antenna array is rotating and the RX array is fixed, the unitary vector $\boldsymbol{u}_r^{\mathrm{SI}}$ can easily be defined in the RX coordinate system as $\boldsymbol{u}_r^{\mathrm{SI}} = [0, -1, 0]^T$. The expression of $\boldsymbol{u}_t^{\mathrm{SI}}$ in the TX coordinate system can then be easily calculated by using the fact that $\boldsymbol{u}_t^{\mathrm{SI}} = -\boldsymbol{R}\boldsymbol{u}_r^{\mathrm{SI}}$, which leads to $\boldsymbol{u}_t^{\mathrm{SI}} = [\sin(\theta_x)\sin(\theta_y), \cos(\theta_x), \sin(\theta_x)\cos(\theta_y)]^T$.

We now evaluate the components of the vectors $\boldsymbol{a}^{(n)}_{t,w'k_h'^{(n)}+h'}$ and $\boldsymbol{a}^{(m)}_{r,wk_h^{(m)}+h}$ in their own coordinate system. Without loss of generality, we assume that both RX and TX arrays have an even number of antennas along the horizontal direction and the vertical direction (*i.e.* $k_h'^{(n)}$, $k_w'^{(n)}$, $k_w^{(m)}$ and $k_h^{(m)}$ are even). We further assume that both k'-th antenna of the TX array and the k-th antenna of the RX array are placed in the top right area of TX and RX so that the coordinates of both $\boldsymbol{a}^{(n)}_{t,w'k_h'^{(n)}+h'}$ and $\boldsymbol{a}^{(m)}_{r,wk_h^{(m)}+h}$ are positive. Note that other locations of the k-th and the k'-th antenna are also possible and this is not impacting the final result. Thus, the coordinates of the vectors $\boldsymbol{a}^{(n)}_{t,w'k_h'^{(n)}+h'}$ and $\boldsymbol{a}^{(m)}_{r,wk_h^{(m)}+h}$ can be written as the following:

$$\boldsymbol{a}^{(n)}_{t,h'k_w'^{(n)}+w'} = \begin{bmatrix} (\frac{k_w'^{(n)}+1}{2} - w')\frac{\lambda}{2} \\ (\frac{k_h'^{(n)}+1}{2} - h')\frac{\lambda}{2} \\ 0 \end{bmatrix}, \tag{17}$$

$$\boldsymbol{a}^{(m)}_{r,hk_w^{(m)}+w} = \begin{bmatrix} (\frac{k_w^{(m)}+1}{2} - w)\frac{\lambda}{2} \\ (\frac{k_h^{(m)}+1}{2} - h)\frac{\lambda}{2} \\ 0 \end{bmatrix}. \tag{18}$$

Substituting (14), (15), (17) and (18) in (13) leads to:

$$\begin{aligned} P_{\mathrm{SI},m}^{\mathrm{PWM}} = & \sum_{n=0}^{N_t^{\mathrm{RF}}-1} \frac{\rho P_{t,n}}{M_t^{(n)} M_r^{(m)}} \\ & \times \Bigg| \sum_{h'=0}^{k_h'^{(n)}-1} \sum_{w'=0}^{k_w'^{(n)}-1} e^{-j\pi(w'\cos(\phi^{(n)})\sin(\theta^{(n)}) + h'\sin(\phi^{(n)}))} \\ & e^{j\pi\sin(\theta_x)\sin(\theta_y)\left(\frac{k_w'^{(n)}+1}{2} - w'\right)} e^{j\pi\cos(\theta_x)\left(\frac{k_h'^{(n)}+1}{2} - h'\right)} \\ & \Bigg(\sum_{h=0}^{k_h^{(m)}-1} \sum_{w=0}^{k_w^{(m)}-1} e^{j\pi(w\cos(\phi^{(m)})\sin(\theta^{(m)}) + h\sin(\phi^{(m)}))} \\ & e^{j\pi\left(\frac{k_h^{(m)}+1}{2} - h\right)} \Bigg) \Bigg|^2. \end{aligned} \tag{19}$$

After some simple arrangements according to the different sum index, (19) becomes:

$$\begin{aligned} P_{\mathrm{SI},m}^{\mathrm{PWM}} = & \sum_{n=0}^{N_t^{\mathrm{RF}}-1} \frac{\rho P_{t,n}}{M_t^{(n)} M_r^{(m)}} \Bigg| \sum_{h'=0}^{k_h'^{(n)}-1} e^{-j\pi h'(\sin(\phi^{(n)}) + \cos(\theta_x))} \\ & \sum_{w'=0}^{k_w'^{(n)}-1} e^{-j\pi w'(\cos(\phi^{(n)})\sin(\theta^{(n)}) + \sin(\theta_x)\sin(\theta_y))} \\ & \sum_{h=0}^{k_h^{(m)}-1} e^{j\pi h(\sin(\phi^{(m)})-1)} \sum_{w=0}^{k_w^{(m)}-1} e^{j\pi w\cos(\phi^{(m)})\sin(\theta^{(m)})} \Bigg|^2. \end{aligned} \tag{20}$$

By using the sum of a geometrical sequences in the different sum operators of (20), we obtain:

$$\begin{aligned} P_{\mathrm{SI},m}^{\mathrm{PWM}} = & \sum_{n=0}^{N_t^{\mathrm{RF}}-1} \frac{\rho P_{t,n}}{M_t^{(n)} M_r^{(m)}} \\ & \times \Bigg| \frac{1 - e^{-j\pi k_h'^{(n)}(\sin(\phi^{(n)}) + \cos(\theta_x))}}{1 - e^{-j\pi(\sin(\phi^{(n)}) + \cos(\theta_x))}} \\ & \frac{1 - e^{-j\pi k_w'^{(n)}(\cos(\phi^{(n)})\sin(\theta^{(n)}) + \sin(\theta_x)\sin(\theta_y))}}{1 - e^{-j\pi(\cos(\phi^{(n)})\sin(\theta^{(n)}) + \sin(\theta_x)\sin(\theta_y))}} \\ & \frac{1 - e^{j\pi k_h^{(m)}(\sin(\phi^{(m)})-1)}}{1 - e^{j\pi(\sin(\phi^{(m)})-1)}} \frac{1 - e^{j\pi k_w^{(m)}\cos(\phi^{(m)})\sin(\theta^{(m)})}}{1 - e^{j\pi\cos(\phi^{(m)})\sin(\theta^{(m)})}} \Bigg|^2. \end{aligned} \tag{21}$$

Then applying Euler's formula yields:

$$P_{\mathrm{SI},m}^{\mathrm{PWM}} = \sum_{n=0}^{N_t^{\mathrm{RF}}-1} \frac{\rho P_{t,n} (k_h^{'(n)} k_w^{'(n)} k_h^{(m)} k_w^{(m)})^2}{M_t^{(n)} M_r^{(m)}} \times \left| \frac{\sin \mathrm{c}(\pi k_h^{'(n)} (\sin(\phi^{(n)}) + \cos(\theta_x)))}{\sin \mathrm{c}(\pi(\sin(\phi^{(n)}) + \cos(\theta_x)))} \frac{\sin \mathrm{c}(\pi k_w^{'(n)} (\cos(\phi^{(n)}) \sin(\theta^{(n)}) + \sin(\theta_x) \sin(\theta_y)))}{\sin \mathrm{c}(\pi(\cos(\phi^{(n)}) \sin(\theta^{(n)}) + \sin(\theta_x) \sin(\theta_y)))} \frac{\sin \mathrm{c}(\pi k_h^{(m)} (\sin(\phi^{(m)}) - 1))}{\sin \mathrm{c}(\pi(\sin(\phi^{(m)}) - 1))} \frac{\sin \mathrm{c}(\pi k_w^{(m)} \cos(\phi^{(m)}) \sin(\theta^{(m)}))}{\sin \mathrm{c}(\pi \cos(\phi^{(m)}) \sin(\theta^{(m)}))} \right|^2. \tag{22}$$

Furthermore, since we consider UPAs with a $\frac{\lambda}{2}$ spacing, ρ can simply be expressed as $\rho = M_r M_t \left(\frac{\lambda}{4D}\right)^2$. By recognizing the Dirichelet kernal in (22), i.e. $\forall a, x \in \mathbb{R}, D_a(x) = sinc(\pi a x)/sinc(\pi x)$ and by remarking that $M_t^{(n)} = k_h^{'(n)} k_w^{'(n)}$ and $M_r^{(m)} = k_h^{(m)} k_w^{(m)}$, the final expression of the received SI power at the m-th RF chain of the RX for the PWM writes:

$$P_{\mathrm{SI},m}^{\mathrm{PWM}} = f(D) \times g_1(\phi^{(m)}, \theta^{(m)}) \times g_2(\phi^{(n)}, \theta^{(n)}, \theta_x, \theta_y), \tag{23}$$

where,

$$f(d) = M_r M_t \left(\frac{\lambda}{4d}\right)^2, \tag{24}$$

$$g_1(\phi^{(m)}, \theta^{(m)}) = \left| D_{k_h^{(m)}}\left(\sin(\phi^{(m)}) - 1\right) D_{k_w^{(m)}}\left(\cos(\phi^{(m)}) \sin(\theta^{(m)})\right) \right|^2, \tag{25}$$

$$g_2(\phi^{(n)}, \theta^{(n)}, \theta_x, \theta_y) = \sum_{n=0}^{N_t^{\mathrm{RF}}-1} P_{t,n} M_t^{(n)} M_r^{(m)} \times \left| D_{k_h^{'(n)}}\left(\sin(\phi^{(n)}) + \cos(\theta_x)\right) D_{k_w^{'(n)}}\left(\cos(\phi^{(n)}) \sin(\theta^{(n)}) + \sin(\theta_x) \sin(\theta_y)\right) \right|^2, \tag{26}$$

with f a function which only depends on the distance between O_{T_x} and O_{R_x}, g_1 a function which only depends on the steering angles of the analog combiner $\boldsymbol{W}_{\mathrm{RF}}$ at RX and g_2 a function which depends on the steering angles of the analog precoder $\boldsymbol{F}_{\mathrm{RF}}$ at TX and the angles of rotation θ_x and θ_y of the TX array. Thus, we have proven that the received SI power can be written as a product of independent functions when the PWM is used. This fact is however not true using the SWM since, in that case, the distance D between the centers would also be an argument of the $\sin \mathrm{c}$ functions in g_2. From this theoretically derivations, we conclude that the assessment of the SI would suffer an approximation and a loss of accuracy using the PWM instead of the SWM. Simulation results of the next section confirm our analysis.

TABLE I
SIMULATION PARAMETERS

Symbol	Value
M_r, M_t	32
N_r^{RF}, N_t^{RF}	4
M_r^{RF}, M_t^{RF}	8
f	28GHz
d	5.36mm
P_t	50W
$\{\phi_r^{(0)}, \theta_r^{(0)}\}$	$\{15°, -45°\}$
$\{\phi_r^{(1)}, \theta_r^{(1)}\}$	$\{-30°, -60°\}$
$\{\phi_r^{(2)}, \theta_r^{(2)}\}$	$\{-30°, 0°\}$
$\{\phi_r^{(3)}, \theta_r^{(3)}\}$	$\{-30°, 60°\}$
$\{\phi_t^{(0)}, \theta_t^{(0)}\}$	$\{10°, 5°\}$
$\{\phi_t^{(1)}, \theta_t^{(1)}\}$	$\{-30°, -45°\}$
$\{\phi_t^{(2)}, \theta_t^{(2)}\}$	$\{-30°, -5°\}$
$\{\phi_t^{(3)}, \theta_t^{(3)}\}$	$\{-30°, 45°\}$

IV. Simulations and Discussion

In this section, simulation results are obtained using a complete simulation chain to evaluate the relevance of the SWM compared to the PWM for the considered MIMO FD system.

A. Simulations parameters

Table I presents the simulation parameters we used. M_x and M_x^{RF} denote the number of elementary antennas of array x ($x \in \{r, t\}$) and the number of elementary antennas per RF chain for array x, respectively. As mentioned before, the two arrays are separated by a distance $d = 5.36$mm, with an operation frequency centered at 28GHz as in the work of [6] and [10]. We assume that each RF chain of the TX array are transmitting signals with the same power fixed at 50W. We further assume that for both arrays, the antennas dedicated to the first RF chain are placed on the top of each array, as the antennas dedicated to the last RF chain are placed on the bottom of each array. Moreover, $\phi_x^{(i)}$ and $\theta_x^{(i)}$ are the elevation and azimuth angles of the i-th RF chain of array x ($i \in \{0, 1, 2, 3\}$). Without additional indications all the following results are obtained with the parameters of Table I.

B. Simulations Results

Note that in all the following figures, the variation of the received SI power regarding the rotation angles θ_x and θ_y represents only the specific case when the different steering angles from Table I are chosen and does not represent a general behavior of the SI power radiation. For other pairs of steering angles the variation may be very different but does not impact our analysis. We first study the influence of the tilt angle θ_x on the received SI power at different RF chains of the RX side

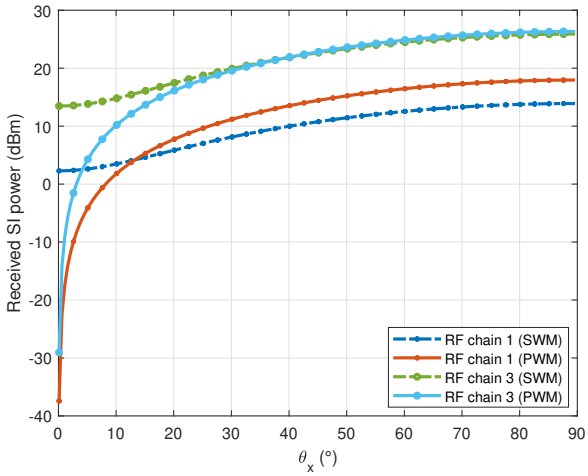

Fig. 2. Comparison between PWM and SWM on the received SI power of the 1st and the 4th RF chain of the RX array by variating θ_x. (Results obtained with only 1 RF chain activated on the TX array).

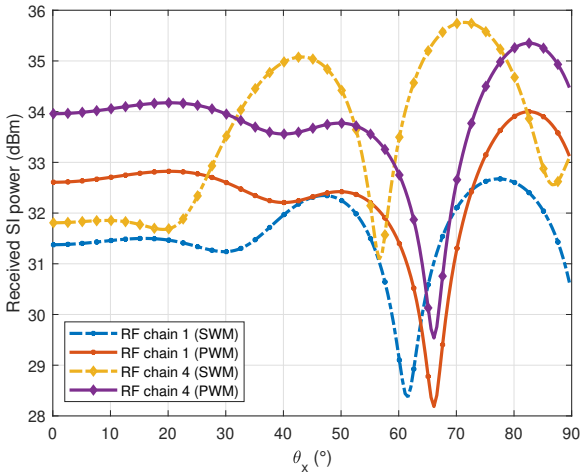

Fig. 3. Comparison between PWM and SWM on the received SI power of the 1st and the 4th RF chain of the RX array by variating θ_x. (Results obtained with 4 RF chains activated on the TX array).

in Fig. 2. In this first series of simulations, we consider that only one of the 4 RF chains of the TX side is activated, and we evaluate the received SI power for all the 4 RF chains of the RX side. For a matter of clarity we decide to show only the results of RF chain #1 and RF chain #4 of the RX side. As shown in Fig. 2, we observe that the received SI power monotonously increases when θ_x increases. This is consistent since the higher the θ_x, the more the RX and TX arrays are in line of sight, thus resulting in an increasing received SI power with a maximum achieved for a perfect face-to-face position of the arrays at $\theta_x = 90°$. Moreover, it is interesting to remark that for the PWM, the received SI power drastically drops when $\theta_x \to 0°$, while the SI power with the SWM is maintained at a non negligible level (superior to 0 dBm) when $\theta_x \to 0°$. Thanks to a better precision of the SWM, we can conclude that in reality the received SI power is less sensitive to the tilt change compared to the approximation offered by the PWM. Both models confirm the intuition that the minimum of SI power is reached for a "perfect" installation of the arrays, *i.e.* $\theta_x = 0°$. However the SWM shows that an installation error up to 5° can be tolerated since the amplitude of the SI power in that case meets very few variation for θ_x varying from 0° to 5°.

In Fig. 3, we study the same metric as in Fig. 2 but considering that all the 4 RF chains are activated on the TX array. This time we study the received SI power at RF chain #1 and #4 of the RX array. As we can observe, since the received SI power is the sum of the contributions of the 4 TX RF chains, there is a larger dynamic variation of the received SI power compared to that reported in Fig. 2. We also observe that even if the PWM is trying to follow the variations of the SWM, there is a clear mismatch of the extremum of the SI power between the two. An important conclusion can be drawn here: for any SIC method based on the estimation of the SI power, a non-negligible estimation error is induced if the PWM is used for the estimation instead of the SWM, thus leading to a poorer performance of the SIC algorithm. Another interesting point is that the received SI power at different RF chains with the PWM have the same variation, with only an amplitude offset between them. The limit of the PWM approximation is clearly shown here: since we showed theoretically in (23) that for the PWM the received SI power is the product of 3 independent functions among which the first one only depends on the distance and the second and the third one only depend on the angles. That means for the same angular variation (θ_x) as in Fig. 3, the received SI power with the PWM is only varying with the distance between O_{R_x} and O_{T_x}. Since RF chain #4 is placed closer to the TX array, this explains the high correlation of variation between the PWMs and their relative position, and further confirms that in the considered situation the SWM is way more precise and accurate than the PWM.

In Fig. 4 we study the same metric as a function of θ_y instead of θ_x, while considering $\theta_x = 0°$. We observe that the SI power with the PWM does not vary according to this rotation change since the planar wave front is not affected by the rotation around the y axis. This result can also be found by replacing θ_x by 0° in (23), which further validates the analysis. On the contrary, the SWM is sensitive to the change and shows in particular that the minimum of SI power is reached when $\theta_y = 0°$, which means when the two a antenna arrays are perfectly coplanar. The same conclusion than before can be made here: it is more relevant to consider the SWM instead of the PWM to model the SI channel.

More generally in Fig. 5, we study the received SI power at the RF chain 4 by variating simultaneously θ_x and θ_y. We observe in particular in Fig. 5-(a) that the received SI power is constant for $\theta_x = 0°$ as we showed previously in Fig. 4, but the SI power with the PWM is still sensitive to θ_y variation for

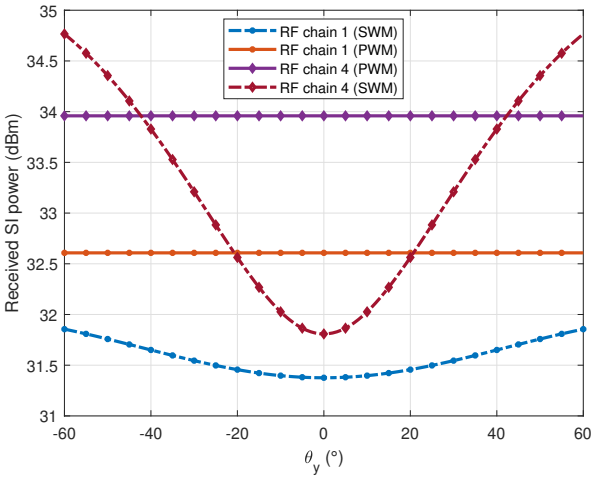

Fig. 4. Comparison between PWM and SWM on the received SI power of the 1st and the 4th RF chain of the RX array by variating θ_y. (Results obtained with 4 RF chains activated on the TX array).

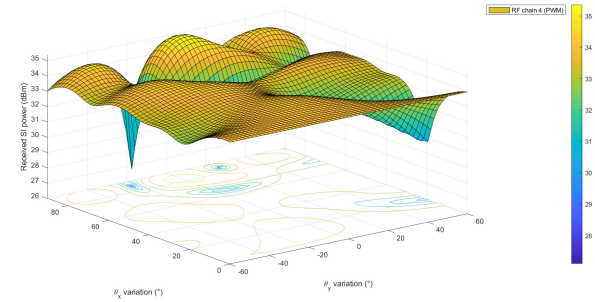

(a) Received SI power at the 4th RF chain of the RX array with PWM by simultaneously variating θ_x and θ_y (Results obtained with 4 RF chains activated on the TX array).

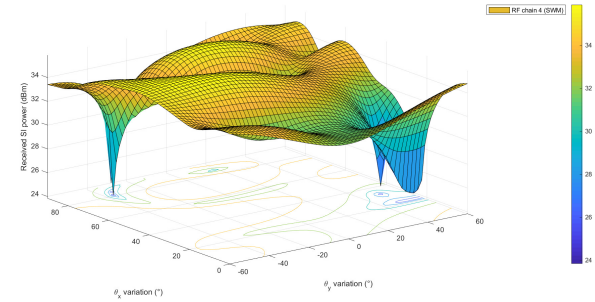

(b) Received SI power at the 4th RF chain of the RX array with SWM by simultaneously variating θ_x and θ_y (Results obtained with 4 RF chains activated on the TX array).

Fig. 5. Comparison of the received SI power at the 4th RF chain with SWM and PWM by simultaneously variating θ_x and θ_y.

other values of θ_x, which approves our theoretical analysis. We observe that the overall variation of the SI power with PWM in Fig. 5-(a) is more monotoneous than the variation with the SWM in Fig. 5-(b), while a clear mismatch between the extremum of SI power for some values of (θ_x, θ_y) can be observed. Once again, the SWM proves to be more relevant than the PWM in the considered situation.

V. Conclusion

In this paper we evaluated and showed the influence of the SWM and the PWM in a MIMO FD system. Indeed, for a generic FD system where the TX array and the RX array are potentially very close to each other, the PWM is no longer viable to model correctly the SI channel. We theorerically proved and highlighted through simulations the limitations of the PWM compared to the SWM. This makes us conclude about the importance of considering the SWM for a more precise model of the SI channel which undoubtedly would lead to much more efficient SIC algorithms.

References

[1] D. Kim, H. Lee, and D. Hong, "A Survey of In-Band Full-Duplex Transmission: From the Perspective of PHY and MAC Layers," *IEEE Commun. Surveys Tuts.*, vol. 17, no. 4, pp. 2017–2046, 2015.

[2] G. Liu, F. R. Yu, H. Ji, V. C. M. Leung, and X. Li, "In-Band Full-Duplex Relaying: A Survey, Research Issues and Challenges," *IEEE Commun. Surveys Tuts.*, vol. 17, no. 2, pp. 500–524, 2015.

[3] H. Alves, T. Riihonen, and H. A. Suraweera, *Full-Duplex Communications for Future Wireless Networks*. Singapore: Springer, 2020.

[4] T. Dinc and H. Krishnaswamy, "Millimeter-wave full-duplex wireless: Applications, antenna interfaces and systems," in *2017 IEEE Custom Integrated Circuits Conference (CICC)*, 2017, pp. 1–8.

[5] A. Sabharwal, P. Schniter, D. Guo, D. Bliss, S. Rangarajan, and R. Wichman, "In-Band Full-Duplex Wireless: Challenges and Opportunities," *IEEE Journal on Selected Areas in Communications*, vol. 32, 11 2013.

[6] A. Bishnu, M. Holm, and T. Ratnarajah, "Performance Evaluation of Full-Duplex IAB Multi-Cell and Multi-User Network for FR2 Band," *IEEE Access*, vol. 9, pp. 72 269–72 283, 2021.

[7] J. Zhang, N. Garg, and T. Ratnarajah, "In-Band-Full-Duplex Integrated Sensing and Communications for IAB Networks," *IEEE Transactions on Vehicular Technology*, pp. 1–14, 2022.

[8] Y. Zhou, "On the performance of spatial modulation and full Duplex radio architectures," Theses, Université de Lyon, Dec. 2021. [Online]. Available: https://tel.archives-ouvertes.fr/tel-03506890

[9] C. K. Sheemar, G. C. Alexandropoulos, D. Slock, J. Querol, and S. Chatzinotas, "Full-duplex-enabled joint communications and sensing with reconfigurable intelligent surfaces," in *Submitted to ArXiV, 19 June 2023*, EURECOM, Ed., 2023, © EURECOM. Personal use of this material is permitted. The definitive version of this paper was published in Submitted to ArXiV, 19 June 2023 and is available at :.

[10] I. P. Roberts, A. Chopra, T. Novlan, S. Vishwanath, and J. G. Andrews, "Spatial and Statistical Modeling of Multi-Panel Millimeter Wave Self-Interference," *IEEE Journal on Selected Areas in Communications*, vol. 41, no. 9, pp. 2780–2795, 2023.

[11] K. Satyanarayana, M. El-Hajjar, P.-H. Kuo, A. Mourad, and L. Hanzo, "Hybrid Beamforming Design for Full-Duplex Millimeter Wave Communication," *IEEE Trans. Veh. Technol.*, vol. 68, no. 2, pp. 1394–1404, 2019.

[12] L. L. Magoarou, A. L. Calvez, and S. Paquelet, "Massive MIMO Channel Estimation taking into account spherical waves," in *2019 IEEE 20th International Workshop on Signal Processing Advances in Wireless Communications (SPAWC)*, 2019, pp. 1–5.

[13] K. T. Selvan and R. Janaswamy, "Fraunhofer and Fresnel Distances: Unified derivation for aperture antennas," *IEEE Antennas Propag. Mag.*, vol. 59, no. 4, pp. 12–15, 2017.

[14] L. C. Yu and M. R. Kamarudin, "Investigation of Patch Phase Array Antenna Orientation at 28GHz for 5G Applications," *Procedia Computer Science*, vol. 86, pp. 47–50, 2016, 2016 International Electrical Engineering Congress, iEECON2016, 2-4 March 2016, Chiang Mai, Thailand.

[15] M. Cai, "Modeling and Mitigating Beam Squint in Millimeter Wave Wireless Communication," Ph.D. dissertation, 03 2018.